Research Article

A novel study of melatonin diffusion in a 3-D cell culture model

Francisco Artime-Naveda[1,2], Lucas Alves-Pérez, David Hevia[1,2,3], Sergio Alcón-Rodríguez[1,2,3], Sheila Fernández-Vega[1,2,3], Alejandro Alvarez-Artime[1,2,3], Isabel Quirós-González[1,2,3], Rafael Cernuda[1,2], Rosa María Sainz[1,2,3,*], Juan Carlos Mayo[1,2,3,*].

[1]Departamento de Morfología y Biología Celular, School of Medicine, University of Oviedo, Asturias, Spain
[2]Instituto Universitario Oncológico del Principado de Asturias (IUOPA), University of Oviedo, Asturias, Spain
[3]Instituto de Investigación Biosanitaria del Principado de Asturias (ISPA), Oviedo, Asturias, Spain.
[*]Correspondence: mayojuan@uniovi.es; sainzrosa@uniovi.es, Tel: +34 985 10 2730

ABSTRACT

Melatonin is now considered a major physiological regulator of many different functions including synchronization of circadian rhythms, antioxidant defense at different levels, immunomodulation, cell growth control, neuroprotector and anti-tumor agent. In addition to its membrane receptor-dependent actions, it has been classically assumed that its diffusion through lipid bilayers contribute to its intracellular actions, including direct and indirect free radical scavenging activities. While pineal gland is the major site of nocturnal production of the indolamine, skin is considered an important source of melatonin synthesis. Here, using a 3-D culture model of HaCaT cells in an artificial scaffold (epidermal equivalents), we have quantified diffusion of melatonin in these cells and compared it to 2-D or spheroid cultures. Diffusion in 3-D scaffold cultures was similar to that found in 2-D culture and proportion of intracellular melatonin was low. AFMK, a major oxidative metabolite of melatonin, was also found and quantified. Redox parameters including total ROS, superoxide or mitochondrial mass were also assayed. We also report the effect of melatonin on the cytoskeleton of normal human keratinocyte HaCaT cells. We propose HaCaT epidermal equivalents as an affordable, easy-to-use, 3-D cell culture tool to test diffusion rates of melatonin but also other similar small molecules. This 3-D models can also be studied at cellular and molecular level, including redox parameters, and can provide important information regarding molecules that can be topically added to skin. Similarly, mechanisms of transportation can also be approached with this methodology.

Key words: Melatonin, AFMK, HaCaT, 3D culture, difussion, epidermal equivalent, ROS

_____

1. INTRODUCTION

The discovery of melatonin in 1958 by Aaron Lerner (1) did certainly not anticipate the extraordinary range of now well-known different functions and cellular mechanisms associated with this tryptophan-derived neuroindolamine. Melatonin is rhythmically secreted exclusively

during the night by the pineal gland (2), but its synthesis in many other tissues and organs is well characterized (3). Furthermore, melatonin production is not restricted to vertebrates, but also occurs in invertebrates and unicellular organisms, including prokaryotes, all of which synthesize this indoleamine (4–6). During the last decade, the presence of melatonin in plants has triggered a great deal of new and interesting discoveries reporting its synthetic machinery (7) as well as numerous functions of the indolamine in higher plants (8).

In addition to its well-known circadian-related functions in adapting the physiology to the light/dark environment and, therefore, to the seasonal changes, particularly in those species who exhibit marked seasonal breeding (e.g., *Mesocricetus auratus*) (9, 10), research during the last 3 decades has highlight melatonin as a potent and versatile antioxidant (11). The antioxidant properties of melatonin have documented its role as a general cytoprotective agent. Furthermore, this indolamine has also been recognized, based on its antioxidant actions, as an anti-proliferative and anti-tumor agent (12) and under certain conditions even as a pro-apoptotic agent for cancer cells (13). Melatonin's oxidative derivatives, i.e., cyclic-3-hydroxy-melatonin (3OHMEL), N^1-acetyl-N^2-formyl-5-methoxykynureamine (AFMK) and N^1-acetyl-5-methoxykynuramine (AMK) as members of a free radical scavenging chain, have also received attention regarding their protective roles (14).

Extra-pineal synthesis results in the presence of melatonin at concentrations higher than those found in nighttime serum; however, the real concentration of melatonin inside cells and its subcellular distribution may vary with the physiological state of the cell. While it has been classically proposed to freely diffuse through phospholipid membranes, to date only a few studies on the interaction between melatonin and lipid bilayers have been reported (15, 16). Additionally, the interactions of melatonin with different proteins have also been documented (17), including GPCR (MT1, MT2) that mediate some of its actions, other receptors (MMP9, PP2A), transporters (GLUT1, PEPT1/2), cytoskeleton proteins (tubulin) and calcium-related proteins (CaM, calreticulin). For pineal-derived melatonin to exhibit intracellular actions at distant sites it may enter cells by one of many ways via simple diffusion.

As to cytoskeleton proteins, they are highly dynamic structures to maintain cellular morphology, facilitate cell movement and intracellular transport, including vesicles or chromosomes during mitosis (18). Therefore, the three major components of cytoskeleton, (19), i.e., actin microfilaments, intermediate filaments, or microtubules, all depend on a highly organized and perfectly coordinated set of binding and regulatory proteins. Among the several factors reported to play a role in this fine regulation, melatonin has been reported as a key element in this dynamic organization [reviewed by (20)]. Banerjee and Margulis suggested that melatonin (0.2 mM) was able to induce mitotic arrest in *Stentor coeruleus* fifty years ago (21). Benítez-king *et al*., were the first to focus on the effect of melatonin on cytoskeletal organization (22), and later Matsui and Machado-Santelli confirmed the effects of melatonin at the physiological level (0.1-1nM) on F-actin (23). While implication of MT1 involvement was early suggested because *mt1* overexpression was necessary for melatonin-induced CHO morphology transformation, surprisingly the effect was achieved only by pharmacological concentrations (0.1 µM) (24). Likewise, physiological level of melatonin alters stress fibers and focal adhesions and neurogenesis, both through Rho-associated kinase and PKC (25, 26). MT2 has also been associated to motility in human mesenchymal stem cells, but again, 1 µM was necessary for triggering this effect (27). Additionally, pharmacological concentrations (1mM) have been successfully used to demonstrate modulation of actin rearrangement in macrophages (28). Finally, considering that melatonin receptors are not required for its effect on cytoskeleton through Ca^{2+}-calmodulin antagonism, its protection against direct free radical damage of cytoskeletal organization and the functions of its metabolites, i.e., kynuramines, which can also antagonize Ca^{2+}-calmodulin (20), it becomes clear that it is necessity of melatonin to crosses lipid bilayers to exert this function inside cells.

A major site of extra-pineal melatonin production is the skin where cells not only produce melatonin but also metabolize it (29, 30). In addition to the 6OH-Mel, other metabolites such as kynuramines, specially AFMK have been detected in HaCaT cells. Currently, human keratinocyte HaCaT cells offer a good model for *in vitro* differentiation and 3D culture, since cultured primary human keratinocytes display a short culture lifetime and subculturing variations (31). Considering the necessity of a 2D-to-3D culture transition (32), HaCaT offers a simple, reliable, low-cost, and easy-to-use method for culturing skin equivalents for clinical purposes (33). Additionally, among several cancer cell lines tested for melatonin diffusion (34), B16F10 murine melanoma cells have been recently shown to display a cytoskeletal structure upon to pharmacological doses of melatonin (35).

The aim of the current study was to assay the potential diffusion and timing of melatonin treatment, using 3D culture model. Considering the numerous evidence demonstrating a key regulatory and antioxidant role of melatonin on skin, our investigations were focused on evaluating the diffusion efficiency of melatonin in a well stablished keratinocyte 3D model employing human HaCat cells and compare it with 2D models in which diffusion has been already assayed. Besides, we also studied the possible occurrence of AFMK, as the major oxidative metabolite. To our knowledge, this is the first study comparing the diffusion of melatonin in both 2D and 3D cultures using LC/MS assays.

2. MATERIALS AND METHODS

2.1. Cell culture.

Murine melanoma B16-F10 cells (# CRL-6475™) and immortalized human epidermic keratinocytes HaCaT (# 300493), purchased from American Type Culture Collection" (ATCC®, Manassas, VA, USA) and from Cell Line Service (CLS, Eppelheim, Germany), respectively and were used. B16-F10 cells were maintained in low glucose DMEM (Dulbecco's Modified Eagle´s Medium, Sigma-Aldrich Inc., St. Louis, MO, USA, # D6046) supplemented with 10% fetal bovine serum (FBS, Corning, Manassas VA 35-089-CV), 1% L-glutamine (Sigma-Aldrich Inc., St. Louis, MO, USA, # G7513), 15 mM HEPES and 1% antibiotic/antimycotic cocktail (penicillin, streptomycin, amphotericin B, Sigma-Aldrich Inc., St. Louis, MO, USA, # A5955). HaCaT were kept as undifferentiated 'naïve' cells by supplementing regular medium with 50 µM EGTA. Both Cell lines were cultured at 37 °C in a humid saturated atmosphere containing 5% CO^2 (Forma™ Steri-Cycle™ i160 CO2, Thermo Scientific™). Medium was changed each other day and cells were regularly subcultured once 90% confluence was reached, using 0.05% trypsin (Gibco®, Grand Island, NY, # 25300-062) for B16-F10 or 0.25% for HaCaT cells. For the indicated experiments, cells were previously counted using a Neubauer chamber and seeded at an initial density of 20,000 cells/ml and then left attach overnight.

2.2. Scaffolds for HaCaT 3D culture as epidermic equivalents.

For the generation of 3D keratinocyte cultures mimicking skin cytoarchitecture, Alvetex™ 3D scaffolds (#AVP005-12, Reprocell, Glasgow, UK) were used. Briefly, 200 mm reticulated polystyrene scaffold with controlled porosity and previously optimized for 3D culture (36) were generated, according to manufacturer's protocol. Scaffolds previously rinsed in 70% ethanol were placed in 6-well plates and covered with 7 ml of complete regular medium and pre-warmed in the CO_2 incubator until cell seeding. Regular medium was then aspirated, and 10^6 cells were seeded in Clonetics® Keratinocyte Growth Medium-2 (KGM®-2; Lonza, CC-3107) at the center of each scaffold insert. After 30 minutes for cell adaptation, 10 ml KGM® medium was added and submerged cells were cultured for 3 additional days and then inserts

were placed into a deep plate for 21 days with 20 ml medium, maintaining the adequate air: liquid interface for promoting differentiation and stratification of keratinocytes, thus mimicking human skin. During this time, 50% media was changed every 3 days. Finally, cultures were washed twice in PBS and inserts were recovered using sterilized tweezers and fixed in OCT under dried ice and kept at -80 °C until processing. Slides obtained with cryostat (Leica CM1900, Leica Microsystems, Wetzlar, Germany) were stained with DAPI to visualize nuclei and examined under the microscope to ensure their viability and histological structure. Micrographs were obtained using a Nikon Eclipse 80i equipped with a Axiocam 712mono camera (Zeiss, Oberkichen, Germany).

2.3. Indolamine permeability assays.

Viable 3D scaffolds were used for permeability assays. After 21 days of culture, inserts were placed in 6-well plates containing sufficient solution (5 ml of HBSS, Sigma-Aldrich Inc., St. Louis, MO, USA, # H9269) to ensure contact with the bottom of scaffold. Additionally, 0.5 ml of HBSS containing melatonin at the indicated concentrations was added on top for 6h (Figure 1). Then, media from both top and bottom sections, were collected and weighed to check a possible volume transfer. At this point, 5-methoxytryptamine (5-MT) was added as HPLC internal standard and liquid samples were kept at -80 °C until analytical assay. Similarly, cells from inserts were washed twice, trypsinized, pelleted and kept at -80 ºC. A small fraction of cells was resuspended in PBS for quantification and standardization.

2.4. Melatonin extraction and LC/MS analysis.

To assay melatonin taken up by cells or melatonin-containing media, a dichloromethane liquid:liquid extraction protocol previously described (37) was used; for this study, 5-methoxytryptophol (5-MT) as an internal standard for estimation of recovery was used. Briefly, cells were resuspended in PBS and one volume of dichloromethane was added and shaken for 10' at RT. After centrifugation at 10,000 xg at 4ºC, organic phase was collected, and the process was repeated. Finally, phases from both extraction cycles were collected, evaporated in a SpeedVac and stored at -80ºC until processing. To this aim, extractions were resuspended in mobile phase (94.6% H_2O, 5,4% acetonitrile, ACN) and analyzed by HPLC-MS/MS (Agilent Technologies, Santa Clara, CA, USA) following a protocol recently stablished (38). Briefly, a C18 column (Eclipse Plus, Zorbax, Agilent technologies) was used and nebulizing gas was set at 7 L/min under 2 bar pressure and 3,5 kV. For melatonin dissociation 13eV collision energy was used, while 17 eV was employed in the case of 5-MT. Selected Reaction Monitoring was the method of choice for mass ion precursor determination in the collision chamber. Simultaneous transitions from $233.1 \rightarrow 174.1$, $265.0 \rightarrow 178.0$ or $192.1 \rightarrow 174.1$ for melatonin, AFMK and 5-MT were respectively monitored, as recently reported (38).

2.5. Free radical assays.

Cryostat sections (10µm) obtained from OCT embedded blocks containing the 3D scaffolds were used for free radical assays. Dihydroethidium (DHE), dihydrorhodamine (DHR), MitoSOX™, MitoTracker™ Red (CMXRos), MitoTracker™ Green and CellROX™ Deep Red were used to detect total cell content of O_2^-, mitochondrial H_2O_2, mitochondrial O_2^-, mitochondria (potential-dependent and independent) or generic ROS, respectively. Sections were placed on Superfrost™ slides, washed in PBS buffer and then incubated with adequate probe dilution (after a previous set up) for 30' in darkness. After washing again with PBS twice, nuclei were counterstained with DAPI, mounted with Fluoromount™ and observed under a Laser Confocal Spectral microscope, Leica TCS-SP8X. Image processing was made with

Fiji/Image J software. Table 1 shows the specific information of the different redox-sensitive fluorescent probes used in the present study.

Table 1. Characteristics of redox-sensitive fluorescent probes.

Probe	[Concentration]	Target
CellROX^TM Deep Red	5.0 µM	Total cytosolic ROS
DHR	10 µM	Total mitochondrial ROS (mainly H_2O_2 y $OONO^-$)
MitoSOX^TM	5.0 µM	Mitochondrial $O_2^{\bullet-}$
MitoTracker^TM Red CMXRos	0.3 µM	Mitochondria, membrane potential dependent
MitoTracker^TM Green FM	0.2 µM	Mitochondria, membrane potential independent

2.6. Phalloidin F-actin staining.

Briefly, cells were cultured on Thermanox^™ coverslides (NUNCTM Brand Products, Rochester, NY, USA) previously placed in 60 mm plates. After the indicated times, coverslides with attached cells were carefully removed with special forceps, placed on slides, washed with PBS and then permeabilized (TBS containing 0.5% Tween-20) for 20'. Then, slides were incubated for 45' at RT with phalloidin (4 µg/mL), counterstained with DAPI, mounted with Fluoromount™ and sealed and observed under the confocal microscope mentioned above.

2.7. Cell viability assays.

HaCaT cells were seeded at 10^4 cells/mL in 100 µL in complete medium in 96 well plates. After the indicated times, cell viability was estimated using the MTT (3-[4,5-dimethylthiazol-2-yl]-2,5 diphenyl tetrazolium bromide) assay and standardized with total DNA content using Hoechst 33258 staining, following protocols previously described (39).

2.8. Statistical analysis.

Experiments were repeated at least 3 times and a representative experiment is plotted. Samples were always analyzed in triplicates and Mean ± SEM is shown in the graphs. For plotting and statistical analysis, GraphPad Prism 9.0.2 software was employed (GraphPad Software, Inc. La Jolla, California, USA). For comparing two independent groups a student 't' test was chosen. For multiple comparations, a Holm-Šídák multiple comparation test was used after one-way ANOVA. In all the cases, a value of $p < 0.05$ was the limit of significance chosen.

3. RESULTS

3.1. Cell type rather than cell culture geometry is critical for explaining melatonin uptake.

B16-F10 and HaCaT were used for both classic 2D and spheroid cultures. Melatonin bioavailability was assayed on these models, using HPLC MS/MS analytical methods. Micrographs of both B16-F10 and HaCaT spheroids are shown in Suppl Figure 1, as well as a typical chromatogram showing the specificity of the melatonin peak. Data on the content of melatonin per 10^6 cells is shown in Table 2. B16-F10 melanoma cells took roughly 1-fold more

melatonin than human HaCaT keratinocytes, whereas the difference in the melatonin content between classic 2D or spheroids is minimal.

Table 2. Content of melatonin (pmol/10⁶ cells) in either, 2D or 3D spheroid cell cultures

CELL TYPE	TYPE OF CULTURE	pmol MELATONIN/10^6 CELLS ± SEM	
		(15')	(60')
B16-F10	2D	1.35 ± 0.33	1.78 ± 0.40
	3D-Spheroids	1.41 ± 0.83	2.90 ± 0.90
HaCaT	2D	0.66 ± 0.16	0.97 ± 0.22
	3D-Spheroids	0.50 ± 0,16	0.84 0.15

3.2. Effects of melatonin on cytoskeleton layout in differentiated HaCaT 2D cultured cells.

It has been already reported that melatonin induces a change in the cytoskeleton in B16F10 melanoma cells (35) and here we have confirmed these changes in this cell type (Suppl Figure 2). When human keratinocyte HaCaT cells were incubated with melatonin, a clear change in the actin cytoskeleton pattern was observed, though these changes were limited to Ca^{2+}-induced differentiated keratinocytes. No clear differences were observed in naïve undifferentiated HaCaT cells (Suppl Figure 3). However, in Ca^{2+} differentiated HaCaT cells, the presence of melatonin induced a marked increase in phalloidin mark, particularly in the cell cortex, where filopodia structures were clearly seen in the cell surface when the indolamine was added to the media (Figure 1). A close-up of these cytoplasmic projections is apparent. Figure 2 displays a detail the filopodia observed in cells incubated with the indolamine in Figure 1. Similar cytoskeleton modulations can be observed in B15F10 cells (Supplement Figure 1), where both, actin and tubulin distribution are altered when melatonin is included in the culture media [for more details, see (35)].
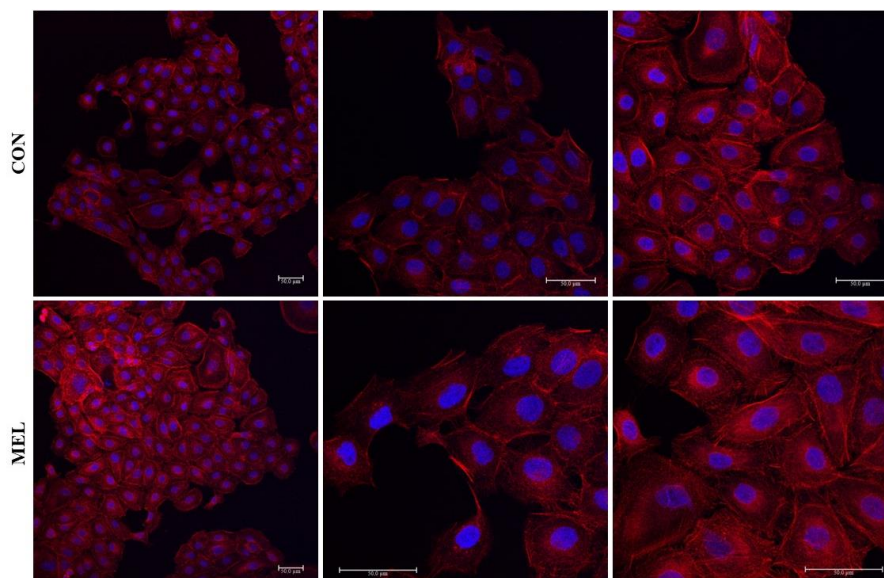

Fig. 1. **Effects of melatonin on changes cytoskeleton layout**.
Confocal microscopy images of Ca2+-differentiated HaCaT human keratinocytes. Left panel, control cells (CON) cultured with vehicle (0.1% DMSO); right panel, 1mM melatonin (MEL) treated cells. Red-conjugated Phalloidin was used to visualize F-actin. Cells were counterstained with DAPI.
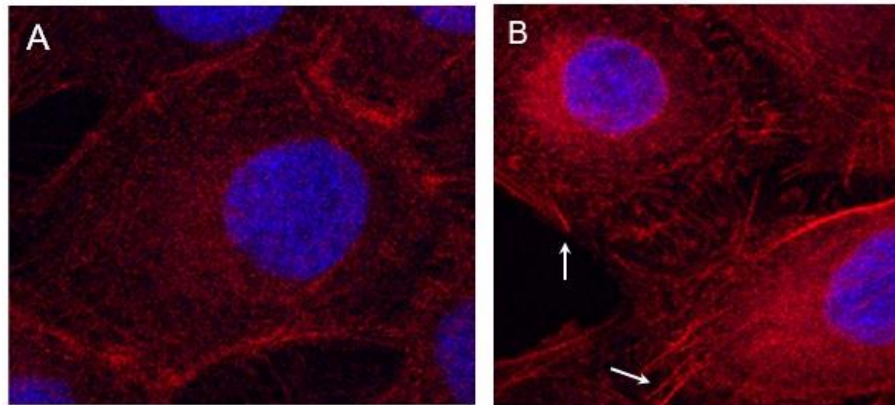
Fig. 2. **A high magnification view of micrographs shown in Figure 1.**
 A, Control cells. B, Melatonin treated cells. Red-conjugated Phalloidin was used to visualize F-actin. Cells were counterstained with DAPI, The arrows indicate actin-based filopodia extensions.

Testing permeability in epidermic equivalents with phenol red-containing media. Spheroids provided a first approach to the question whether melatonin can equally reach cells in a 3D model and yet, this cell culture technique does not allow for the analysis of melatonin permeability in a much better controlled epidermal environment. To this aim, the epidermal equivalents using HaCaT 3D scaffolds made on Alvetex™ was constructed. Phase contrast and confocal micrographs confirmed the correct cytoarchitecture of the scaffolds (Figure 3).
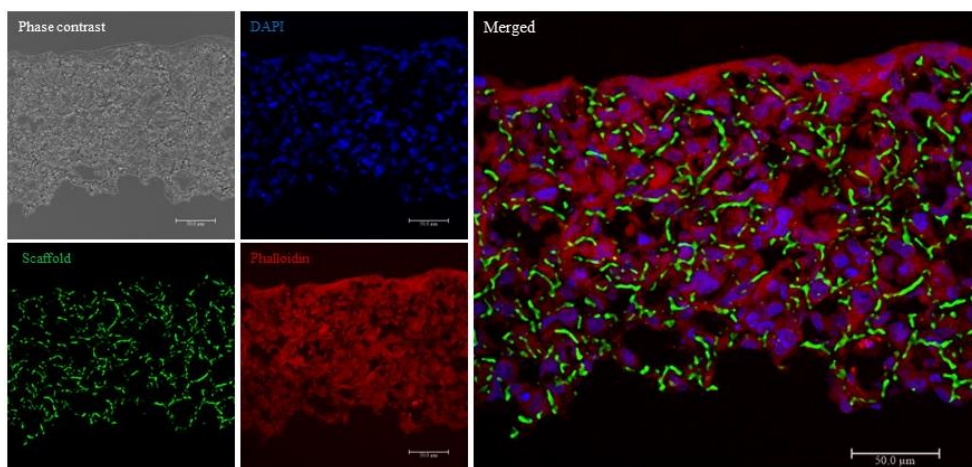

Fig. 3. **The cytoarchitecture of the HaCaT 3D scaffolds**.
 Alvetex™ scaffolds showing human keratinocyte HaCaT epidermic equivalents. A. phase contrast image of HaCaT grown on the scaffold. B. bright phase contrast images corresponding to the artificial scaffold were digitally converted into green for visualizing the supporting material. C. DAPI stained nuclei. D. Red-conjugated phalloidin was used to visualize the F-actin filaments. E, merged image used to show cell continuity.

To determine whether the epidermal equivalents were continuous at the cellular level without pores that would allow the passage of small molecular weight substances, a phenol red diffusion assay was performed. To this end, 100 µl of media containing phenol red was added on top of the scaffolds and the possible passage of phenol red to the bottom media was monitored. Phenol red presence was checked in bottom media by spectrometry. As it is shown (Figure 4), the positive control (HBSS) displayed a clear peak at 557nm, corresponding with

the maximal wavelength absorbance of phenol red. On the contrary, negative control using DMEM media w/o phenol red did not displayed a detectable peak at this wavelength. Finally, both control as well as samples incubated with melatonin showed small traces of phenol red (Figure 4). Spectrophotometric assay of the phenol red present in bottom wells confirmed that up to a 25% of diffusion of this substance through the epidermal equivalent which could not be attributed to cell-controlled diffusion.
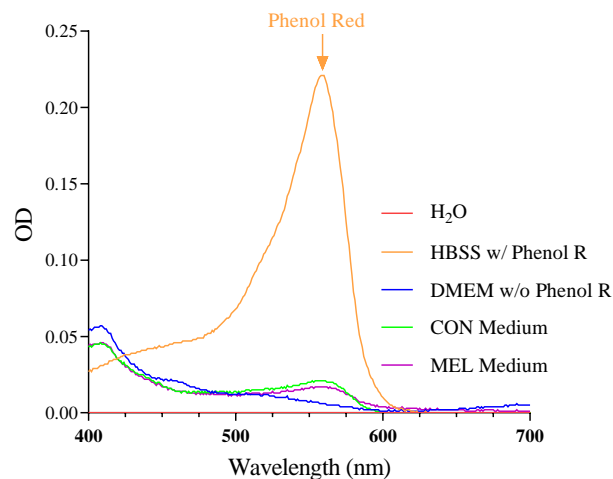

Fig. 4. Spectrophotometric analysis of phenol red.
The samples were Hanks's Balanced Salt Solution (HBSS) containing phenol red, Dulbecco's Modified Eagles Medium without phenol red as well as representative samples used in the study of control medium (CON) or melatonin treated medium (MEL) from the bottom of Alvetex™ scaffolds containing the diffused substances added on top. A scan of absorbance profile between 400-700 nm is shown. Phenol red shows a peak at 557 nm. Water was used as negative control.

3.3. Chromatographic analysis of melatonin and AFMK.

Analytical measurement of melatonin and its oxidative metabolite, AFMK by LC-MS/MS analysis was performed for either control or melatonin-treated HaCaT 3D scaffold samples (Figure 5). Supplementary Figure 2 shows that the three compounds, i.e., AFMK, 5-MT (internal standard) as well as melatonin were all resolved at 4.1, 6.8 and 7.4 min, respectively in all the samples assayed. Negative control with no melatonin addition (Figure 5A) displays a clear peak at 6.8 min, corresponding to the internal standard, 5-MT, as well as a chromatographic signal at 7.4 min, compatible with a minimal amount of detectable melatonin present in control serum. However, levels of melatonin detected in samples incubated with this indolamine were almost 300-fold higher (Figure 5).

HaCaT 3D scaffolds were treated with 1, 10 or 500 µM of melatonin and results with the quantification of melatonin and AFMK in both cell inserts (located on top) and in media present in bottom wells are shown in Figure 5A and 5B, respectively. The amount of both melatonin and AFMK increased exponentially with the concentration of melatonin employed. Thus, the net amount of melatonin found in bottom media (diffused) was between 2.4 to 22 times higher, but this increase was greater when low concentrations (1-10 µM) of melatonin were assayed. Similar results were obtained with AFMK, with an increase between 3 and 60 times in diffusion. Again, the increase was much higher when low concentrations of the indole were used (1-10 µM), suggesting a saturation effect in the diffusion and/or uptake. The ratios of melatonin and AFMK detected in bottom wells *vs* inserts, as well as the quantity of both

substances per 10^6 cells in 500 µM treated epidermic equivalents are shown in Figure 6 and Table 3.
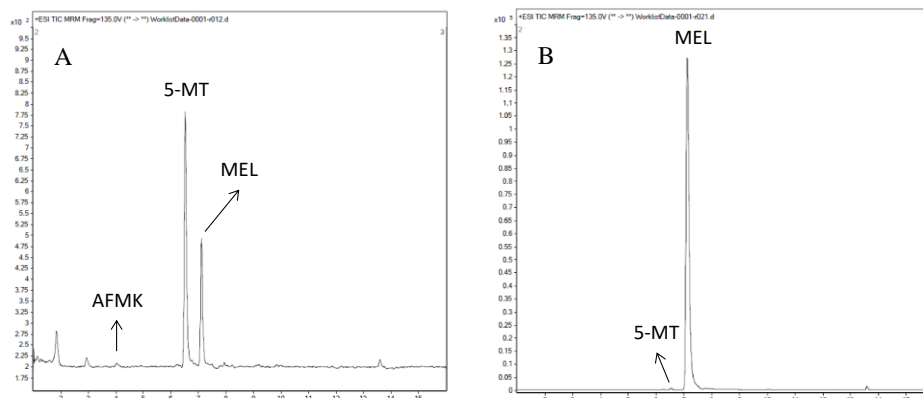

Fig. 5. The effects of HaCaT 3D scaffolds on melatonin penetration and metabolism.
Representative chromatograms of control (A) or melatonin treated (B) samples showing the elution profiles AFMK, 5-MT and melatonin, with retention times of 4.1, 6.8 and 7.4 min., respectively. A minimal amount of melatonin was detected in control samples (5x102 peak) but scale shown on B is 3 orders higher (5x102 vs 1.3 x 105 peaks, respectively).
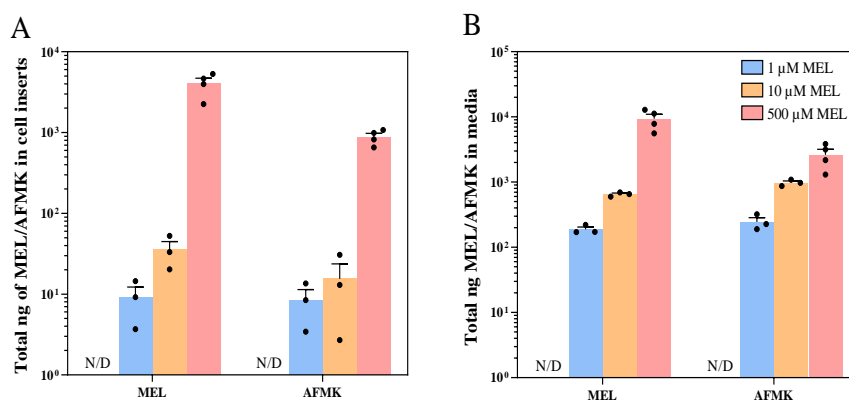

Fig. 6. The ratios of melatonin to AFMK in HaCaT 3D scaffolds culture.
The ratios of melatonin to AFMK detected in inserts (A) or in bottom plates media (B), corresponding to intracellular vs diffused, respectively, in control or in melatonin treated samples (1, 10 or 500 µM). Neither Melatonin nor AFMK were detected in control samples (N/D).

Table 3. Ratio of melatonin/AFMK (%) detected in bottom wells (diffused) vs inserts and pmol melatonin/AFMK detected, standardized with number of cells.

[Mel] added (µM)	Ratio (%) in wells *vs* inserts		pmol in inserts		pmol/10^6 cells[1]	
	MEL	AFMK	MEL	AFMK	MEL	AFMK
1	95.38 / 5.16	96.66 / 3.34	39.18 ± 13.38	32.11 ± 11.05	-	-
10	94.84 / 4.61	98.44 / 1.55	152 ± 40.47	58.60 ± 30.95	-	-
500	69.84 / 30.16	74.74 / 25.24	17.43 ± 2.82	3.35 ± 0.35	11.28 ± 4.45	14.60 ± 2.14

3.4. Redox assays of melatonin treated HaCaT epidermic equivalents.

Once the presence of melatonin and AFMK were identified in the epidermal equivalents, along with the diffusion of melatonin through the 3D structure, our next aim was to check whether this uptake/diffusion was associated with redox changes within the cells. To this end, several different redox probes were used with the results being shown in Figure 7. The generic oxidative stress-response probes show no difference in the formation of free radicals between control and melatonin-treated epidermal equivalents (Figure 7A and B). While specific mitochondrial superoxide production tested with MitoSox™ showed a slight increase in melatonin-treated equivalents. The mitochondria-specific probes exhibited a reduction in the net mitochondrial mass (Figure 7D) with no changes in membrane potential (Figure 7E), thus documenting a net increase in the ratio in both situations (Figure 7F), indicating the presence of a significantly higher mitochondrial membrane potential in melatonin-treated cells.
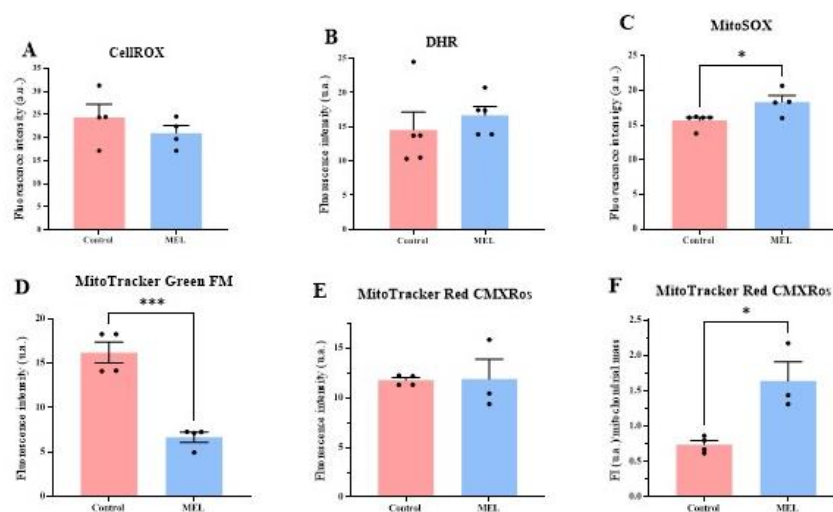

Fig. 7. Effects of melatonin on redox status of HaCaT epidermic equivalents.

Redox parameters assayed in control or melatonin-treated (MEL) HaCaT epidermic equivalents grown on Alvetex™ scaffolds, using specific probes. A, Total cytosolic ROS (CellROX); B, total mitochondrial ROS (DHR); C, mitochondrial $O_2^{-}\bullet$ (MitoSOX); D, membrane potential-independent mitochondrial mass (MitoTracker™ Green), E, membrane potential-dependent mitochondrial mass (MitoTracker Red); F, ratio of membrane potential-dependent vs mitochondrial mass.

4. DISCUSION

In the present study we have assessed the ability of melatonin to penetrate into two different types of spheroids using either, HaCaT or B16F10 cells, finding very similar uptake rates when compared with 2D matched cultures. In addition, we have shown how melatonin is able to cross a 3D culture human skin model, namely HaCaT epidermal equivalents, in which this indolamine was taken up by cells and react with ROS, therefore producing detectable amounts of one of the main melatonin oxidative metabolites, i.e., AFMK. The present study demonstrates the utility of this 3D cell culture model for assaying diffusion and bioavailability of small molecules such as melatonin. Furthermore, considering the important role of the indolamine in skin, we have demonstrated that addition of melatonin on these epidermic equivalents allow it to enter and potentially react with free radicals inside cells, therefore changing the intracellular redox status.

Different from other small hydrophobic molecules, including steroid hormones or other non-polar substances, the amphiphilic nature of melatonin has been classically used to explain its ability to cross lipid bilayers, either plasma or organelle membranes, and therefore, exhibit the wide range of functions. This seems to be especially important for explaining the intracellular antioxidant properties. Not only does melatonin appears in sera but it can also be detected in many other body fluids, including saliva, milk, sperm, or amniotic fluid. The distribution is not, however, homogeneous throughout the body, which would explain the necessity of other more specific, likely protein-mediated transporters accounting for such difference (40).

Analytical assays of specific ability to interact and/or cross artificial bilayers of melatonin have generated different results. Pioneering works from Costa and co-workers showed a preferential position of melatonin in the surface of dimyristoylphosphatidylcholine (DMPC) artificial membranes, but according to these studies, quenching of melatonin fluorescence was higher in the hydrophobic region, confirming presence of this molecule in among the hydrophobic tails of phospholipids (15, 41). This melatonin interaction with DMPC membranes apparently increases fluidity (42). Using zwitterionic dipalmitoyl phosphatidylcholine (DPPC) multilamellar liposomes (MLVs), Severcan *et al*. have shown the effect of melatonin on lipid phase transition and the increase in lipid dynamics, pointing also to a high presence of melatonin in the central region of bilayers (43) which helps to explain melatonin's ability to reduce lipid peroxidation (44). More recently, using two different, low and high, concentrations of melatonin in DMPC membranes and analyzing bilayers using 2D X-ray diffraction, Dies *et al*. have shown that while low concentrations of melatonin (0.5 mol%) are arranged in melatonin-enriched patches, a higher content of melatonin (30 mol%) induces a parallel alignment to the bilayers (45), which agrees with previous evidences showing that melatonin interacts with both, membrane surface and with the hydrophobic tail. Nevertheless, Marti and Lu have recently reported the comparative study of the interaction between melatonin, serotonin, or tryptophan with phospholipid membranes. Though authors show that cholesterol alters this interaction, particularly in the case of melatonin, the study confirmed that the cost of energy for melatonin access the center of the membrane is high (40 kJ/mol), with diffusion rates of 10^{-7} cm^2/s (46). Transition of melatonin in puro DMPO membranes is low, but increasing concentrations of cholesterol improves this movement (16). The stabilization effect of melatonin on membranes from both nanometer and micrometer-size liposomes described by Bolmatov *et al*. (47), thus preserving lipid domains, strengths the hypothesis that melatonin might interact rather than cross lipid bilayers.

Beyond the issue of passive diffusion through the lipid bilayer, there have been aims to study melatonin diffusion in cells and tissues in 3D models, similar to the one employed in this study. In a non-pathologic model similar to the HaCaT epidermal equivalents assayed here, Bae and Cols have successfully employed the pineal indolamine in dermal papilla spheroids, also using pharmacological concentrations similar to those used here, showing an increase in proliferation and in diameter in the spheroids in a dose-dependent manner (48). Even though the interest of this study was focused on the mediation of AKT/GSK3β/β-Catenin in this effect, the results show that pharmacological doses of melatonin change the cell fate, likely mediated by redox-related mechanisms rather than by membrane receptors. No apparent morphological changes were found in melatonin-treated HaCaT 3D epidermal equivalents, but 2D analysis showed a clear impact on keratinocyte cytoskeleton, with the formation of protrusions and filopodia-like structures. However, depending on the morphology and on the biochemical partners of actin filaments, filopodia may be involved in different processes (49). Here, actin reorganization is associated with a decrease in HaCaT proliferation (data not shown) and concomitant with a clear display of F-actin around the cell cortex. Whether these morphological changes of actin are related with the establishment of new cell junctions should

be further studied. A clear impact of melatonin on B16F10 melanoma cells cytoskeleton has also been reported, along with a reduction in cell proliferation, an increase in melanin but with no effect on metastasis (35), which might indicate a function of melatonin on certain cytoskeletal components. Other attempts for clarifying melatonin effects on 3D cultures have been made, particularly on breast, glioblastoma, colon, or lung cancer spheroids/organoids (50–53).

Results have shown melatonin diffusion through cells in 3D models in the range of previously assayed in 2D cultures (37). However, to discard intercellular diffusion, phenol red (MW=354.4) was used for standardization of net diffusion of small non-polar molecules like melatonin. Therefore, using this substance added in the culture media on top of the Alvetex™ 3D scaffolds chamber, the amount of phenol red detected on the bottom of cell plates was then determined. By use of this method, it was estimated a basal phenol red diffusion of roughly 25% (data not shown), but, nevertheless whether phenol red diffuses between or through cells cannot be inferred from our results. Thus, the possibility of melatonin being taken up by cells and passed to other neighboring cells cannot be ruled out, as the cellular continuity in the scaffold is apparent (see Figure 3E). However, in this regard, melatonin (or phenol red) diffusion between cells, through intercellular junctions cannot be excluded either. Thus, tight junctions, which usually exert a "fence and gate" barrier (54), are also involved in the so-called paracellular transport, major responsible for the transepithelial ionic diffusion. Other non-hydrophilic, low molecular weight molecules could also be transported through a transepithelial mechanism (55), likely mediated by claudins (56). Nevertheless, though this type of transport has been extensively studied in the renal tubules and gut epithelium, the relative importance in other epithelia remains unclear.

Regarding the redox control of melatonin, we describe for the first time the potential conversion of melatonin into its main oxidative metabolite, i.e., AFMK, as the kynuramine was detected in either 2D or 3D cultures of HaCaT cells after melatonin addition. The amounts of AFMK analyzed are comparable to those of melatonin and the ratio of AFMK detected in inserts (epidermic equivalents) significantly increased when the indolamine was added at the highest concentration, which could indicate an oxidative conversion. However, we failed to demonstrate an antioxidant action of the indolamine, since no difference in total ROS (CellROX) or mitochondrial superoxide (MitoSOX) were observed. Interestingly, melatonin treated cells showed a lower mitochondrial mass but with a higher membrane potential (see Figure 7F). Whether these results indicate that the conversion of melatonin into the kynuramine is redox-independent or not, should be further evaluated since several enzymes or cytochrome C also can convert melatonin to AFMK.

As a general conclusion, we here show that human keratinocytes forming 3D epidermic equivalents can be used as an easy and affordable cell culture model for studying diffusion of melatonin in skin cells. By extension, the model can also be employed to study the interaction of small molecules and how they behave in contact with skin. Melatonin diffuses through the epidermic cells in the 3D model, though the intracellular concentrations reached are small compared to the amounts added to the culture. Conversion into AFMK is feasible in the epidermic equivalents, but the antioxidant activity still remains to be further demonstrated by induce oxidative stress in this model.

5. CONCLUSIONS AND LIMITATIONS OF THE STUDY

While the phenol red demonstrates basal diffusion of small molecules, considering the close cell:cell interactions observed in the 3D model, intercellular vs intracellular diffusion should be further studied in this model. Also, more accurate studies are needed for testing redox probes

in this specific model, which would help to stablish this Alvetex™ 3D models as potential in vitro standards for assaying diffusion of small molecules and their interaction with skin.

Finally, it is noteworthy to mention that other cell models, including human normal keratinocytes and human melanoma cells, might be of great interest as alternative cellular models, to recreate a more realistic environment to test diffusion. These models, which offer other limitations, would provide insights into new drugs availability for human keratinocytes.

ABREVIATIONS

AKT/PKB: Protein kinase B
AFMK: N^1-acetyl-N^2-formyl-5-methoxykynuramine
AMK: N^1-acetyl-5-methoxykynuramine
DHE: Dihydroethidium
DHR: Dihydrorhodamine
GLUT1/SLC2A1: Glucose Transporter 1/Solute carrier family 2 member 1
GPCR: G-protein Coupled Receptors
GSK3β: Glycogen synthase kinase 3 beta
MEL: Melatonin
MitoSOX™: Mitochondria Superoxide indicator
MMP9: Matrix metalloproteinase 9
MT1/2: Melatonin Receptor ½
PEPT1/2: Oligopeptide transporter ½
PP2A: Phosphatase protein 2A
ROS: Reactive Oxygen Species

ACKNOWLEDGEMENT

AUTHORSHIP

R.M.S. and J.C.M were responsible for conceptualization and writing. F.A.N and L.A.P performed most of the experiments and processed data. D.H and F.A.N. assisted with analytical techniques. S.A.R. and S.F.V assisted with spheroid cultures. A.A.A. helped with B16F10 cultures. I.Q.R. helped setting up Alvetex® culture and tissue processing. R.C. oversaw micrographs, fluorescence and confocal microscopy and photo edition.

CONFLICT INTEREST

Authors declare no conflict of interest.

REFERENCES

1. Arendt J, Lerner A (2007) Who discovered melatonin. *J. Pineal Res* **43**: 106–107?
2. Reiter RJ (1991) Pineal melatonin: Cell biology of its synthesis and of its physiological interactions. *Endocr. Rev.* **12**: 151–180.
3. Huether G (1993) The contribution of extrapineal sites of melatonin synthesis to circulating melatonin levels in higher vertebrates. *Experientia* **49**: 665–670.
4. Vivien-Roels B, Pévet P (1993) Melatonin: presence and formation in invertebrates. *Experientia* **49**: 642–647.
5. Schippers KJ, Nichols SA (2014) (Deep, dark secrets of melatonin in animal evolution. *Cell* **159**, 9–10.
6. Hardeland R, Poeggeler B (2003) Non-vertebrate melatonin. *J. Pineal Res.* **34**: 233–241.
7. Tan DX, Reiter RJ (2020). An evolutionary view of melatonin synthesis and metabolism related to its biological functions in plants. *J. Exp. Bot.* **71**: 4677–4689.
8. Arnao MB, Hernández-Ruiz J (2015) Functions of melatonin in plants: a review. *J. Pineal Res.* **59**: 133–150.
9. Reiter RJ (1993) The melatonin rhythm: both a clock and a calendar. *Experientia* **49**: 654–664.
10. Dardente H (2012) Melatonin-dependent timing of seasonal reproduction by the pars tuberalis: pivotal roles for long daylengths and thyroid hormones. *J. Neuroendocrinol.* **24**: 249–266.
11. Galano A, Tan DX, Reiter RJ (2018) Melatonin: A versatile protector against oxidative DNA damage. *Molecules* **23**.
12. Mayo JC, *et al.* (2017) IGFBP3 and MAPK/ERK signaling mediates melatonin-induced antitumor activity in prostate cancer. *J. Pineal Res.* **62**: 1–17.
13. Sainz RM, Lombo F, Mayo JC (2012) Radical decisions in cancer: Redox control of cell growth and death. *Cancers (Basel)* **4**: 442–474.
14. Galano A, Tan DX, Reiter RJ (2013) On the free radical scavenging activities of melatonin's metabolites, AFMK and AMK. *J. Pineal Res.* **54**: 245–257.
15. Costa EJX, Lopes RH, M. Lamy-Freund T (1995) Permeability of pure lipid bilayers to melatonin. *J. Pineal Res.* **19**: 123–126.
16. Lu H, Marti J (2020) Cellular absorption of small molecules: free energy landscapes of melatonin binding at phospholipid membranes. *Sci. Rep.* **10**: 1–12.
17. Liu L, Labani N, Cecon E, Jockers R (2019) Melatonin target proteins: too many or not enough? *Front. Endocrinol. (Lausanne)* **10**: 791.
18. Fletcher DA, Mullins RD (2010) Cell mechanics and the cytoskeleton. *Nature* **463**: 485–492.
19. Mostowy S, Cossart P (2012) Septins: the fourth component of the cytoskeleton. *Nat. Rev. Mol. Cell Biol*. **13**: 183–194.
20. Benítez-King G (2006) Melatonin as a cytoskeletal modulator: Implications for cell physiology and disease. *J. Pineal Res.* **40**: 1–9.
21. Banerjee S, Margulis L (1973) Mitotic arrest by melatonin. *Exp. Cell Res.* **78**: 314-318.
22. Benítez-King G, Huerto-Delgadillo L, Antón-Tay F (1990) Melatonin effects on the cytoskeletal organization of MDCK and neuroblastoma N1E-115 cells. *J. Pineal Res.* **9**: 209–220.
23. Matsui DH, Machado-Santelli GM (1997) Alterations in F-actin distribution in cells treated with melatonin. *J. Pineal Res.* **23**: 169–175.
24. Witt-Enderby PA, *et al.* (2000) Melatonin induction of filamentous structures in non-neuronal cells that is dependent on expression of the human mt1 melatonin receptor. *Cell Motil. Cytoskeleton* **46**: 28–42.

25. Bellon A, Ortíz-López L, Ramírez-Rodríguez G, Antón-Tay F, Benítez-King G (2007) Melatonin induces neuritogenesis at early stages in N1E-115 cells through actin rearrangements via activation of protein kinase C and Rho-associated kinase. *J. Pineal Res.* **42**: 214–221.

26. Ramírez-Rodríguez G, Ortiz-López L, Benítez-King G (2007) Melatonin increases stress fibers and focal adhesions in MDCK cells: participation of Rho-associated kinase and protein kinase C. *J. Pineal Res.* **42**: 180–190.

27. Lee SJ, Jung YH, Oh SY, Yun SP, Han HJ (2014) Melatonin enhances the human mesenchymal stem cells motility via melatonin receptor 2 coupling with Gαq in skin wound healing. *J. Pineal Res.* **57**: 393–407.

28. Kadena M., *et al.* (2017) Microarray and gene co-expression analysis reveals that melatonin attenuates immune responses and modulates actin rearrangement in macrophages. *Biochem. Biophys. Res. Commun.* **485**: 414–420.

29. Slominski AT, *et al.* (2017) Melatonin, mitochondria, and the skin. *Cell. Mol. Life Sci.* **74**: 3913–3925.

30. Kim TK, *et al.* (2013) Metabolism of melatonin and biological activity of intermediates of melatoninergic pathway in human skin cells. *FASEB J.* **27**: 2742–2755.

31. Colombo I, *et al.* (2017) HaCaT cells as a reliable in vitro differentiation model to dissect the inflammatory/repair response of human keratinocytes. *Mediators Inflamm.* **2017:** 7435621.

32. Jensen C, Teng Y (2020) Is it time to start transitioning from 2D to 3D cell culture? *Front. Mol. Biosci.* **7**: 33.

33. Jung MH, Jung SM, Shin HS (2016) Co-stimulation of HaCaT keratinization with mechanical stress and air-exposure using a novel 3D culture device. *Sci. Rep.* **6**: 33889.

34. Hevia D, *et al.* (2015) Melatonin uptake through glucose transporters: A new target for melatonin inhibition of cancer. *J. Pineal Res.* **58**: 234–250.

35. Alvarez-Artime A, *et al.* (2020) Melatonin-induced cytoskeleton reorganization leads to inhibition of melanoma cancer cell proliferation. *Int. J. Mol. Sci.* **21**: 548.

36. Bokhari M, Carnachan RJ, Cameron NR, Przyborski SA (2007) Novel cell culture device enabling three-dimensional cell growth and improved cell function. *Biochem. Biophys. Res. Commun.* **354**: 1095-1100.

37. Hevia D, *et al.* (2008) Melatonin uptake in prostate cancer cells: Intracellular transport versus simple passive diffusion. *J. Pineal Res.* **45**: 247–257.

38. Fernández AS, *et al* (2022) Evaluation of different internal standardization approaches for the quantification of melatonin in cell culture samples by multiple heart-cutting two dimensional liquid chromatography tandem mass spectrometry. *J. Chromatogr. A* **1663**: 462752.

39. Quiros-Gonzalez I, *et al.* (2022) Androgen-dependent prostate cancer cells reprogram their metabolic signature upon GLUT1 upregulation by manganese superoxide dismutase. *Antioxidants (Basel)* **11**: 313.

40. Mayo JC, Sainz RM, González-Menéndez P, Hevia D, Cernuda-Cernuda R (2017) Melatonin transport into mitochondria. *Cell. Mo. Life Sci.* **74**: 3927–3940.

41. Costa EJX, Shida CS, Biaggi MH, Ito AS, Lamy-Freund MT (1997) How melatonin interacts with lipid bilayers: A study by fluorescence and ESR spectroscopies. *FEBS Lett.* **416:** 103–106.

42. Saija A, *et al.* (2002) Interaction of melatonin with model membranes and possible implications in its photoprotective activity. *Eur. J. Pharm. Biopharm.* **53**: 209–215.

43. Severcan F, Sahin I, Kazanci N (2005) Melatonin strongly interacts with zwitterionic model membranes-evidence from Fourier transform infrared spectroscopy and differential scanning calorimetry. *Biochim. Biophys. Acta Biomembr.* **1668**: 215–222.

44. García JJ, *et al.* (2014) Protective effects of melatonin in reducing oxidative stress and in preserving the fluidity of biological membranes: A review. *J. Pineal Res.* **56**: 225–237.
45. Dies H, Cheung B, Tang J, Rheinstädter MC (2015) The organization of melatonin in lipid membranes. *Biochim. Biophys. Acta Biomembr.* **1848**: 1032–1040.
46. Martí J, Lu H, (2021) Microscopic interactions of melatonin, serotonin and tryptophan with zwitterionic phospholipid membranes. *Int. J. Mol. Sci.* **22**: 1–25.
47. Bolmatov D, *et al.* (2019) Deciphering Melatonin-stabilized phase separation in phospholipid bilayers. *Langmuir* **35**: 12236–12245.
48. Bae S, *et al.* (2022) Melatonin increases growth properties in human dermal papilla spheroids by activating AKT/GSK3β/β-Catenin signaling pathway. *PeerJ* **10**: e13461.
49. Jacquemet G, Hamidi H, Ivaska J (2015) Filopodia in cell adhesion, 3D migration and cancer cell invasion. *Curr. Opin. Cell Biol.* **36**: 23–31.
50. Sokolov D, *et al.* (2022) Melatonin and andrographolide synergize to inhibit the colospheroid phenotype by targeting Wnt/beta-catenin signaling. *J. Pineal Res.* **73**: e12808.
51. Phiboonchaiyanan PP, *et al.* (2021) Melatonin and its derivative disrupt cancer stem-like phenotypes of lung cancer cells via AKT downregulation. *Clin Exp. Pharmaco.l Physiol.* **48**: 1712–1723.
52. Jadid MFS, *et al.* (2021) Melatonin increases the anticancer potential of doxorubicin in Caco-2 colorectal cancer cells. *Environ. Toxicol.* **36**: 1061–1069.
53. Zhao Y, Wang C, Goel A (2022) A combined treatment with melatonin and andrographis promotes autophagy and anticancer activity in colorectal cancer. *Carcinogenesis* **43**: 217–230.
54. Garcia MA, Nelson WJ, Chavez N (2018) Cell-cell junctions organize structural and signaling networks. *Cold Spring Harb Perspect Biol.* **10**: a029181.
55. Wang L, Ding L, Du Z, Liu J (2020) Effects of hydrophobicity and molecular weight on the transport permeability of oligopeptides across Caco-2 cell monolayers. *J. Food Biochem.* **44**: e13188.
56. Nagarajan SK, Klein S, Fadakar BS, Piontek J (2023) Claudin-10b cation channels in tight junction strands: Octameric-interlocked pore barrels constitute paracellular channels with low water permeability. *Comput. Struct. Biotechnol. J.* **21**: 1711–1727.